A pseudo-Lagrangian method for remapping ocean biogeochemical tracer data: Calculation of net Chl-a growth rates

Alain de Verneil, Peter J. S. Franks

AGU PUBLICATIONS

JGR

Journal of Geophysical Research: Oceans

RESEARCH ARTICLE

10.1002/2015JC010898

Key Points:
- Pseudo-Lagrangian transformation produces corrected spatial maps of Chl-a
- Advection of Chl-a provides a spatial map of net growth rates
- Application to biogeochemical data expands the number of rate measurements

Correspondence to:
A. de Verneil,
adeverne@ucsd.edu

Citation:
de Verneil, A., and P. J. S. Franks (2015), A pseudo-Lagrangian method for remapping ocean biogeochemical tracer data: Calculation of net Chl-a growth rates, *J. Geophys. Res. Oceans*, *120*, 4962–4979, doi:10.1002/2015JC010898.

Received 2 APR 2015
Accepted 17 JUN 2015
Accepted article online 19 JUN 2015
Published online 18 JUL 2015

A pseudo-Lagrangian method for remapping ocean biogeochemical tracer data: Calculation of net Chl-a growth rates

Alain de Verneil[1] and Peter J. S. Franks[1]

[1]Scripps Institution of Oceanography, University of California, San Diego, La Jolla, California, USA

Abstract A key goal in understanding the ocean's biogeochemical state is estimation of rates of change of critical tracers, particularly components of the planktonic ecosystem. Unfortunately, because ship survey data are not synoptic, it is difficult to obtain spatially resolved estimates of the rates of change of tracers sampled in a moving fluid. Here we present a pseudo-Lagrangian transformation to remap data from underway surveys to a pseudo-synoptic view. The method utilizes geostrophic velocities to back advect and relocate sampling positions, removing advection aliasing. This algorithm produces a map of true relative sampling locations, and allows for determination of the relative locations of observations acquired along streamlines, as well as a corrected view of the tracer's spatial gradients. We then use a forward advection scheme to estimate the tracer's relative change along streamlines, and use these to calculate spatially resolved, net specific rates of change. Application of this technique to Chlorophyll-a (Chl-a) fluorescence data around an ocean front is presented. We obtain 156 individual estimates of Chl-a fluorescence net specific rate of change, covering ~1200 km^2. After incorporating a diffusion-like model to estimate error, the method shows that the majority of observations (64%) were significantly negative. This pseudo-Lagrangian approach generates more accurate spatial maps than raw survey data, and allows spatially resolved estimates of net rates of tracer change. Such estimates can be used as a rate budget constraint that, in conjunction with standard rate measurements, will better determine biogeochemical fluxes.

1. Introduction

The concentrations of biogeochemical properties in the ocean emerge from an ever-changing balance of the local rates of production and loss. For example, phytoplankton concentration is controlled by its growth rate, which is a function of nutrients and light, and loss rates, which include such processes as grazing, viral lysis, and natural mortality. In addition to these physiological and trophic rates, local phytoplankton concentrations are affected by dynamics such as sinking and active swimming. Unfortunately, all these rates are difficult to measure. Furthermore, these dynamics all occur within the context of a moving medium, making the study of planktonic ecosystems and associated biogeochemical fluxes a discipline that must necessarily resolve complex biological interactions within physical flows.

A general equation to describe the time evolution of concentration C of a biogeochemical property at a fixed location is:

$$\frac{\partial C}{\partial t} + \mathbf{u} \cdot \nabla C = Diffusion + Swimming + Sources - Sinks \quad (1)$$

The advection term $\mathbf{u} \cdot \nabla C$ on the left-hand side (LHS) of (1) appears as a result of taking the full time derivative of C: in a fixed, Eulerian coordinate frame, the quantity C and its spatial gradients move with the flow. If one transforms to a Lagrangian frame that moves with the flow, the advection term disappears since water velocity relative to the coordinate is now zero:

$$\frac{dC}{dt} = Diffusion + Swimming + Sources - Sinks \quad (2)$$

Transforming to a Lagrangian frame (2) therefore simplifies (1) by removing the effects of advection on the LHS, leaving in situ biological rates, diffusion, and swimming on the right-hand side (RHS) to

determine the local rate of change of concentration (note now that the partial derivative of C has become full in equation (2)). Many studies make use of this fact in their sampling strategy: they measure both rates and tracer concentrations in particular water masses by following drifters or adding conservative inert tracers (e.g., *Wilkerson and Dugdale* [1987], *Abbott et al.* [1990], *Law et al.* [1998], and all FeAX's noted in *Boyd et al.* [2007], *Li et al.* [2008], *Jickells et al.* [2008], and *Landry et al.* [2009]). Indeed, various algorithms, tools, and software have been developed to optimize a ship's ability to follow a water mass during biogeochemical experiments [*Doglioli et al.*, 2013, and references within]. However, most biological rate measurements in the ocean are difficult to obtain, often coming from isolated observations that are necessarily extrapolated to be representative of dynamics within larger-scale features.

Here we present a "pseudo-Lagrangian" data analysis technique that transforms underway survey data from an Eulerian to a Lagrangian frame, allowing for explicit quantification of the RHS of (1), and thus calculation of in situ net rates of tracer concentration change. The approach begins with the construction of a spatial map of the Eulerian velocity field in the survey region. Then, we find multiple streamlines of the Eulerian flow that allow us to remove the effects of advection along these trajectories. We use these trajectories with measured tracer concentrations of (in this case) Chlorophyll-a (Chl-a) fluorescence to create a Lagrangian field by back advecting the tracer along the trajectories, similar to reverse domain filling techniques [*Dragani et al.*, 2002; *Methven et al.*, 2003]. We then analyze this Lagrangian field to quantify the net rates of change due to the RHS of (1). Creating Lagrangian trajectories from Eulerian data is not a novel concept: similar approaches have been applied to create better estimates of atmospheric tracer fields and modeling of rates [*Sutton et al.*, 1994; *Nilsson and Leck*, 2002; *Dragani et al.*, 2002; *Taylor*, 1992; *Bowman et al.*, 2013], and many ocean studies analyze Lagrangian trajectories derived from Eulerian output of satellite data or ocean models [*Blanke and Raynaud*, 1997; *d'Ovidio et al.*, 2004; *Doglioli et al.*, 2006; *Lehahn et al.* 2007; *Lett et al.* 2008; *d'Ovidio et al.*, 2010]. Indeed, SeaSoar data similar to ours have been advected using a comparable methodology to this study, but with the objective of evaluating sampling biases of dynamical variables [*Allen et al.*, 2001; *Rixen et al.*, 2001, 2003]. However, limited physical data sets and the general difficulty of measuring biological tracers have precluded application of this technique to the evolution of actual in situ tracer data in the ocean (though for a satellite-derived estimation of phytoplankton net growth rate, see *Abbott and Zion* [1985]). Our method is not truly Lagrangian because there are details of the flow that are not resolved at small scales, and its applicability relies upon the presence of a dominant, stationary velocity field. The term "pseudo-Lagrangian" is chosen to reflect use of in situ data in calculating rates, similar to *Nilsson and Leck* [2002], though it should not be confused with the "pseudo-Lagrangian" data assimilation technique [*Molcard et al.*, 2003].

Lagrangian drifters designed to follow water masses typically only approximate Lagrangian measurements, and must factor in "slippage" (though see *D'Asaro* [2003] and *D'Asaro et al.* [2011]). Still, floats and drifters with telemetry have become relatively inexpensive for physical Lagrangian studies, allowing for synoptic coverage over large spatial regions. These studies, over multiple deployments, have yielded estimates of flow structure and other physical quantities of interest, and have created an entire field of Lagrangian statistics (see *LaCasce* [2008] for a recent review). By contrast, the instruments and techniques for measuring biological variables usually require more intense and continued effort, limiting both the spatial and temporal scales at which these observations are made. Without an environmental context, many biological data are collected in a relative vacuum, creating problems for the analysis of the dynamics underlying patchiness of plankton communities and their associated biogeochemical fluxes [*Powell and Okubo*, 1994; *Martin*, 2003; *Bracco et al.*, 2000; *Koszalka et al.*, 2007]. With the pseudo-Lagrangian approach, we hope to begin to address this contextual issue in field data.

In this study, we develop the pseudo-Lagrangian methodology within the context of an ocean front. We diagnose the physical flow field from underway SeaSoar vertical profiles and acoustic Doppler current profiler (ADCP) currents, outlined in section 2. Then, with use of an Eulerian-Lagrangian coordinate transformation in section 3, we create a pseudo-Lagrangian tracer field using Chl-a fluorescence. In section 4, we describe how the tracer field can be used to estimate large-scale, spatially resolved rates, which would be difficult to obtain in any other way. Section 5 discusses the results and conclusions of this rate application, and section 6 concludes with suggestions of future uses of this approach.

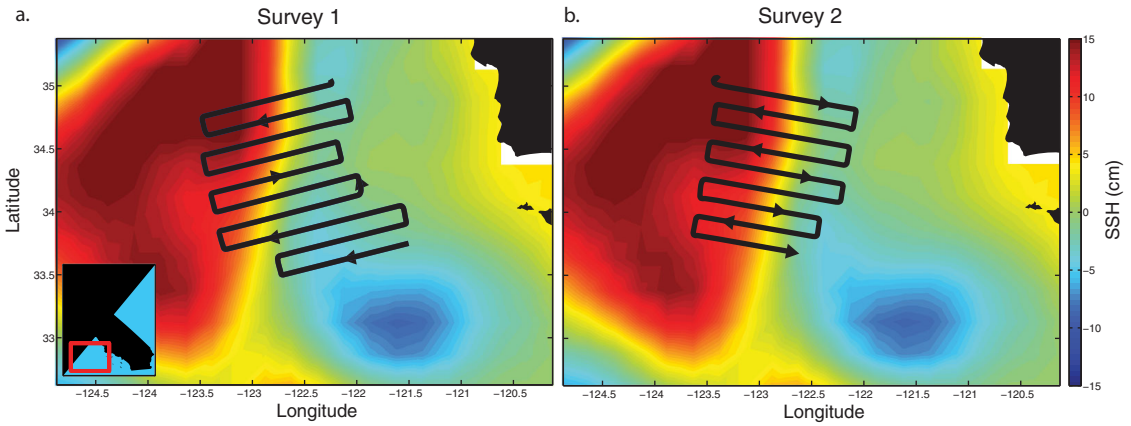

Figure 1. E-front. Aviso Sea surface height anomaly average for (a) Survey 1 (July 29 to August 3) and (b) Survey 2 (21–25 August 2012). Black line shows the location and direction of the survey relative to the frontal feature.

2. Data

2.1. Sampling Plan and Context

Data for this study derive from the 2012 process cruise (P1208), dubbed "E-Front," of the NSF-funded California Current Ecosystem (CCE) Long Term Ecological Research (LTER) program conducted from July to August 2012 aboard *R/V Melville*. The purpose of the cruise was to identify regions of enhanced horizontal physical and biological gradients (i.e., fronts) and quantify their role in the pelagic ecosystems of the CCE. The study region spans a roughly rectangular area with (123.8°W, 33.5°N) and (121.5°W, 35°N) delineating diagonal corners. As indicated by Aviso satellite sea level anomaly data (Figure 1), a frontal region existed in the vicinity of two mesoscale features: cyclonic to the southeast and anticyclonic to the west. The altimeter products were produced by Ssalto/Duacs and distributed by Aviso, with support from CNES (http://www.aviso.altimetry.fr/duacs/). At the onset of the cruise, E-Front's hydrographic structure was surveyed in a radiator pattern by SeaSoar from 30 July to 3 August going south to north, moving upstream relative to the geostrophic jet. Subsequent to this survey, biological measurements and process experiments were conducted at various locations in relation to the frontal region (similar to *Landry et al*. [2009]). After these biological measurements, another SeaSoar survey was performed from 21 August to 25 August moving downstream relative to the geostrophic jet to ascertain the final position of the feature.

2.2. SeaSoar and Alf-A Data

During both hydrographic surveys, the SeaSoar conducted profiles in a tow-yo fashion. Data were acquired by two onboard SeaBird SBE-9Plus CTDs (Sea-Bird Electronics, www.seabird.com), a Seapoint SCF Chl-a fluorometer (Seapoint Sensors, Inc., www.seapoint.com), Wet Labs C-Star transmissometer (Western Environmental Technologies, www.wetlabs.com), and Rinko-III oxygen sensor (Rockland Oceanographic Services, Inc., www.rocklandocean.com). All data were sampled at 24 Hz. Temperature and conductivity data were lag corrected to minimize salinity spiking, though thermal inertia lag [*Lueck and Picklo*, 1990] was ignored due to the flushing rate of the SeaSoar [see *Rudnick and Luyten*, 1996]. These data were then averaged into a 1 Hz time series, followed by a 6 m resolution vertical binning to give single up and down casts, approximately 8 min apart with ∼2 km horizontal displacement. Density data were then constrained to obey static stability [*Rudnick*, 1996] using a constrained linear least squares algorithm (MATLAB and Optimization Toolbox Release 2012a, The Mathworks, Inc., Natick, Massachusetts, USA).

SeaSoar-derived Chl-a fluorescence measurements were matched with surface measurements concurrently from an Advanced Laser Fluorometer (ALF-A) developed by A. Chekalyuk (Lamont Doherty Earth Observatory, www.ldeo.columbia.edu). The ALF-A measures laser-stimulated excitation (LSE) of fluorescence at multiple wavelengths in flow-through sampling [*Chekalyuk and Hafez*, 2008]. Data collected during E-Front were compared with and calibrated by in situ chlorophyll extractions. The correlation between SeaSoar fluorescence and ALF-A chlorophyll is high, with a linear relationship explaining 98% of the variance in nighttime measurements and 95% overall. In general, the ratio of fluorescence to chlorophyll is not constant.

However, after accounting for nonphotochemical quenching, the skill in predicting chlorophyll improves [*Chekalyuk and Hafez*, 2011]. Based on the ALF-A data, the largest nonphotochemical quenching (NPQ) effect at the surface amounted to at most 23% of the surface signal, and presumably decreased exponentially with depth [*Krause and Weis*, 1991; *Müller et al*., 2001]. This NPQ effect was found to be a minor contribution to the variability in the Chl-a and rate estimates used later, so the estimate of Chl-a is reliable (section 4). Weak NPQ is not surprising, as satellite coverage during E-Front suffered from strong cloud cover, indicative of reduced overall insolation. Thus, variability in the fluorescence-derived Chl-a due to NPQ has been ignored in this study.

2.3. ADCP Currents

Vertical profiles of horizontal velocity were obtained from the shipboard-mounted 75 kHz Ocean Surveyor ADCP on the *R/V Melville*. The UHDAS preprocessed data were averaged into 15 min ensembles with a 16 m vertical bin resolution [*Firing and Hummon*, 2010]. Subsequently, the angle of misalignment was recalculated from the total measured and ship velocities in a linear variance minimization scheme to provide estimates of the water velocities [*Rudnick and Luyten*, 1996].

2.4. Objective Maps

Density, Chl-a, and ADCP currents were objectively mapped onto matching horizontal grids at specific depths using the methodology of *Le Traon* [1990]. The signal distribution was assumed Gaussian, with correlation length scales determined from the observed autocovariance calculated from binned data. These lengths are 25, 55, 25, 15 km in x and 45, 25, 55, 30 km in y directions for density, ADCP u velocity, ADCP v velocity, and Chl-a fluorescence, respectively. In determining error, a noise-to-signal ratio of $\leq$0.05 is assumed, and all values used in subsequent calculations were restricted to an error threshold of 0.1 [*Rudnick and Luyten*, 1996]. Objective fits for density assume a planar mean and a single valued mean for currents, in concordance with geostrophy. Chl-a fluorescence was not assumed to conform to any particular functional form and by default is assigned a single mean value (Figure 2). The objective map grids have a resolution of $\sim$4 km on each side, to reduce overinterpolation between adjacent sampling locations, and to include sufficient resolution between survey lines.

2.5. Geostrophic Currents

All velocity fields used in this study are geostrophic currents fit to the objectively mapped density and ADCP data through a L_2 norm misfit minimization scheme. After application of a static stability criterion to the three-dimensional density field, geostrophic currents are found via a relaxation method [*Rudnick*, 1996] solving:

$$\nabla^2\psi = H^{-1}(\nabla^2 R + \zeta) \tag{3}$$

where ψ is the stream function, a depth-integrated scalar for the water volume under consideration. H is defined by

$$H = \int_{z_1}^{z_2} w_u dz \tag{4}$$

where w_u is a weighting parameter reflecting confidence in the velocity observation, and is here kept equal to one, essentially making H the depth. R is the quantity

$$R = \frac{g}{f\rho_0}\int_{z_0}^{z} \rho dz \tag{5}$$

Finally, ζ is the relative vorticity found from the ADCP objective map. All these quantities are depth integrated from the shallowest ADCP depth at 27 m to a 300 m reference level. Geostrophic velocities are found from the relations

$$u_g = -\frac{\partial\psi}{\partial y} + \frac{\partial R}{\partial y} \tag{6}$$

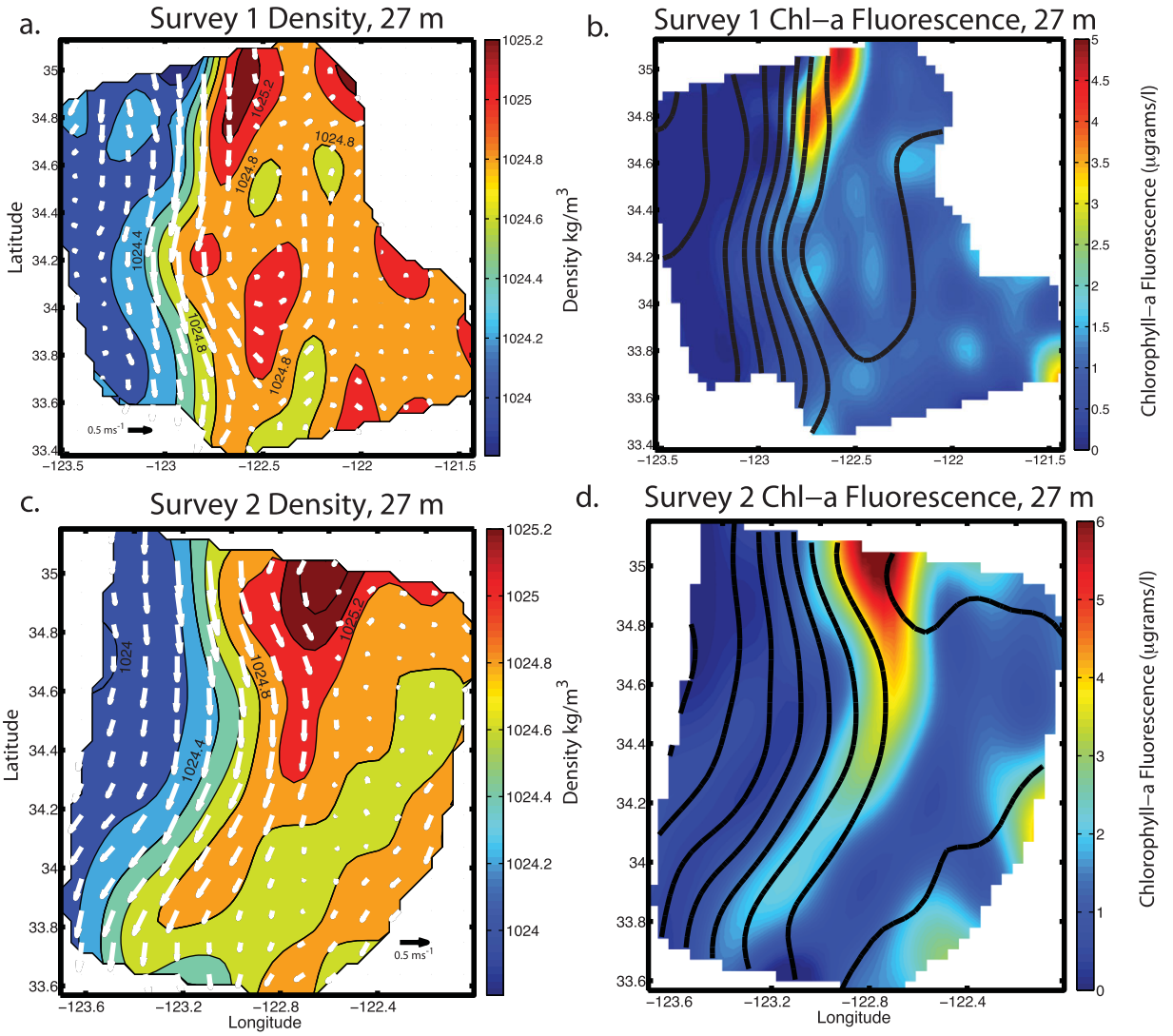

Figure 2. Objective maps of (a and c) Density and (b and d) Chlorophyll-a fluorescence for Surveys 1 and 2, at 27 m depth. White arrows in Figures 2a and 2c indicate the horizontal currents, displayed at one-fourth resolution. Black contours in Figures 2b and 2d show the streamlines of the flow. Note the strong, stationary frontal feature in both density and Chl-a.

$$v_g = \frac{\partial \psi}{\partial x} - \frac{\partial R}{\partial x} \tag{7}$$

The geostrophic currents account for the majority of the variance in the objectively fit ADCP currents, with a vector complex correlation of 0.84 (Figure 2). As noted in *Rudnick* [1996], the vertical velocity shear, and not the geostrophic current, is constrained to be isopycnal; even so, the geostrophic current largely follows isopycnals.

Following *Viúdez et al.* [2000], we can determine the relative error in our currents as the divergent portion of the ADCP objective map, reflecting aliased phenomena not removed by objective analysis. After solving for these components via a similar relaxation method, we arrive at a divergent velocity error distribution that is approximately lognormal, similar to theory and observations of turbulent motion in the ocean [*Kolmogorov*, 1962; *Gurvich and Yaglom*, 1967; *Yamazaki and Lueck*, 1990]. As might be expected [*Pallàs-Sanz et al.*, 2010], introducing these errors randomly into (3) produces little change in the stream function. The resulting displacements lead to equivalent eddy diffusivities of O(1–10) $m^2\ s^{-1}$, which are an order of magnitude lower than the "diffusivity" used for error in section 4. We thus forego including variance of the advective geostrophic velocity field for this analysis.

Given that this study was conducted around a front, we chose the balanced geostrophic currents as the leading-order contribution to the dynamics of the flow field. We could include ageostrophic vertical

motions in our analysis. Vertical velocities are inferred via the omega equation through adoption of quasi-geostrophic dynamics [*Hoskins et al*., 1978]. After solving this equation, however, the magnitudes of vertical velocities in the region have maxima at ∼3 m/d, with most areas producing displacements within the bin size of our data at the time scales used for our analyses O(1–3 days). We therefore ignore vertical velocities in this study, and only use the horizontal, geostrophic currents.

3. Pseudo-Lagrangian Method

One difficulty in analyzing data acquired during underway surveys is that during the survey, the tracer will move along streamlines. Subsequent spatial maps of the tracer necessarily include this advection along streamlines, thus confounding the quantification of the true spatial gradients. The pseudo-Lagrangian approach takes the spatial maps of the tracer and back advects the tracer along the streamlines to their original positions when the survey began. To do this, it is necessary to have a well-resolved, stationary flow field with which to define the streamlines. Each tracer sample is advected back along the streamline for the amount of time between the start of the survey and the given observation, using the velocities along the streamline. The resulting pseudo-Lagrangian spatial map shows the spatial distribution of the tracer as it would have appeared synoptically at the start of the survey. This pseudo-Lagrangian map can then be used to calculate net rates of change of the tracer, as we show below.

3.1. Assumptions

The pseudo-Lagrangian transformation entails application of Eulerian velocity fields to convert a surveyed tracer distribution into a pseudo-Lagrangian distribution by removing the effects of advection. Assumptions implicit to this methodology are: (a) the physical flow field is known and stationary for the length of time under consideration, and (b) the structure of the tracer field moving with the flow is larger than the minimum sampling resolution, i.e., the tracer spatial autocovariance length scale is larger than spacing between observations.

In this study, the first assumption is met: both SeaSoar surveys, spaced a month apart, yield leading-order balanced geostrophic currents that explain the majority of observed velocity field variance (Figure 2). The two velocity fields display similar magnitudes and spatial patterns, making the temporal window of a ∼3–4 day survey synoptic relative to dynamic changes in the physical flow field. We note that objective mapping was applied to smooth over high-frequency phenomena inevitably aliased within the data set, such as internal waves, surface gravity wave-induced Stokes drift, and tidal flow [*Kunze and Sanford*, 1984; *Whitt and Thomas*, 2013; *McWilliams and Fox-Kemper*, 2013]. In a sense, then, the maps represent a spatial and temporal averaging. Generally speaking, time-averaged Eulerian and Lagrangian fields do not produce equivalent velocities [*Andrews and McIntyre*, 1978] and yield different trajectories. Here we assume that the geostrophic current field at this front is leading order and stationary, and we ignore higher-order nonlinear contributions to the flow. In a further attempt to justify geostrophy, we performed our forward advection algorithm (described in section 4) on a tracer that should be conserved: salinity. Comparing the abilities of the raw ADCP data, objectively mapped ADCP data, and fit geostrophic velocities in conserving salinity, they all performed in a qualitatively similar manner (not shown), though the geostrophic velocities did marginally better. As an additional note, the geostrophic currents also produced the most successful survey line crossings, the necessary condition to calculate net rates of change in the tracer field in our subsequent analysis. This post hoc method of validating one's chosen velocity may be useful in future applications of the pseudo-Lagrangian method.

Regarding the second assumption, here we use Chl-a fluorescence as the tracer of interest. The observed spatial autocovariance length scales across the front (15 km) are larger than the distance between successive vertical profiles (∼2 km), while along-front autocovariance length scales (30 km) are again larger than spacing between SeaSoar survey lines (∼20 km). Given this result, we assume that the tracer field between survey locations varies continuously and monotonically, and that finer-scale features are relatively unimportant.

3.2. Procedure

Having satisfied the assumptions, we apply the pseudo-Lagrangian transformation (Figure 3). Initially, we start with the tracer distribution as surveyed, namely with concentration values at discrete locations on

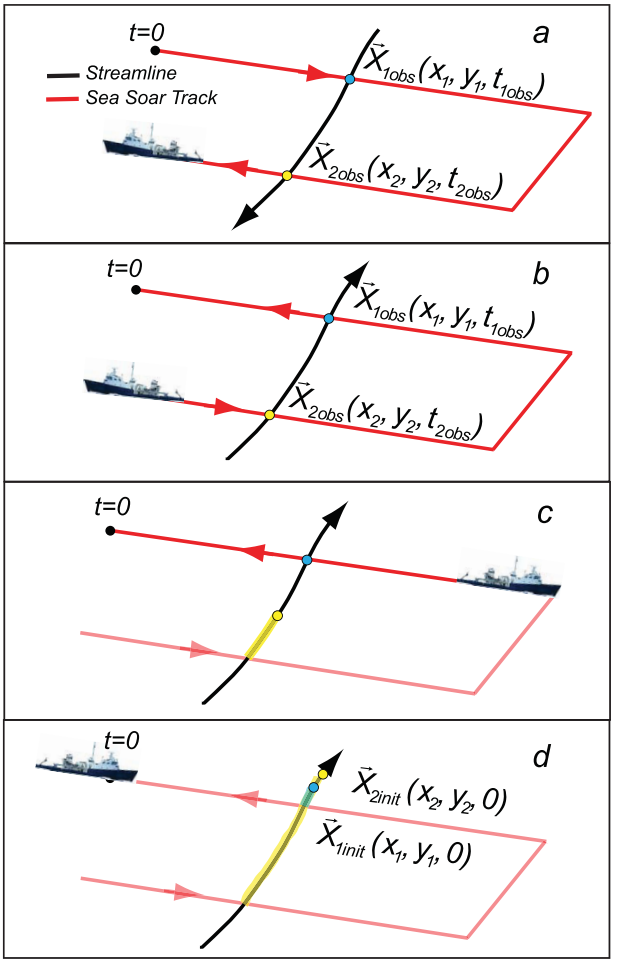

Figure 3. Pseudo-Lagrangian procedure. (a) Streamlines of flow are calculated from the survey data. Observations on the same streamline are identified. (b) Flow direction is reversed, and the survey time is reversed. (c) Positions are back advected for a time t_{obs} from their sampling, to arrive at their inferred initial location (d). Note that a particle sampled later along a streamline can arrive at an initial position upstream of a particle sampled earlier, depending on the flow and the ship's survey speed.

streamlines generated from the geostrophic flow (Figure 3a). Discrete sampling locations can be considered to be the Lagrangian position at the time of observation, $\mathbf{X}_{obs}=\mathbf{X}(x, y, t_{obs})$. To calculate Lagrangian positions via integration of the velocity field, we set the reference time $t = 0$ to be at the start of the survey, with $\mathbf{X}_{init}=\mathbf{X}(x, y, 0)$. Knowing the time elapsed between the survey start and each observed tracer profile, t_{obs}, we now can solve for each tracer's initial location (at the start of the survey) using the Eulerian velocity field. In this notation, the equation for the time-dependent tracer location $\mathbf{X}_{obs}$ is

$$\mathbf{X}_{obs}=\mathbf{X}_{init}+\int_0^{t_{obs}}\mathbf{U}(x, y, t)|_{(x,y)=\mathbf{X}(x,y,t)}dt \quad (8)$$

We seek $\mathbf{X}_{init}$, which we find by subtracting the particle's trajectory from its observed location $\mathbf{X}_{obs}$. This equates to a backward advection of the observed position $\mathbf{X}_{obs}$ along its streamline to $\mathbf{X}_{init}$ over a time t_{obs} (Figures 3b and 3c). While simple in form, note that the velocity value in (8) is evaluated at time-varying positions along the streamline that depend on the velocity, complicating its analytical solution. We overcome this problem by approximating the integral as a discrete sum:

$$\mathbf{X}_{init}=\mathbf{X}_{obs}-\sum_{n=0}^{t_{obs}/\Delta t}\mathbf{U}(x, y, t=n\Delta t)\cdot\Delta t \quad (9)$$

where the velocity becomes the value at the recursively calculated position. We implemented this integration with a simple first-order Euler numerical scheme, with $\Delta t \approx 5$ min, well within the CFL stability criterion. Velocity values were interpolated from the objectively mapped velocity using inverse-square distance weighting [*Shepard*, 1968]. The accuracy of the method was tested using sequential back and forward time-integration, yielding locations nearly identical to the profile locations.

The results of this procedure are the data positions where they would have been at the beginning of the survey, $t = 0$ (Figure 3d). This is the pseudo-Lagrangian transformation, removing the aliasing due to advection, to present the true, synoptic relative positions of neighboring data profiles at the start of the survey. Note that samples acquired later in the survey could potentially have initially been *upstream* of samples acquired earlier, if the water velocities moved the sampled water downstream faster than the ship surveyed the current (Figure 3d). In this situation, the pseudo-Lagrangian-reconstructed ship track will cross itself, giving multiple samplings of the same water parcel.

3.3. Analysis of Transformed Map

Having produced the transformed pseudo-Lagrangian positions of the sample data, we can now interpret the "corrected" distribution of our tracer. A sequence of back advected positions for SeaSoar Survey 2 Chl-a fluorescence data (Figure 4) shows that while the velocity field is geostrophic and nondivergent, and should not allow for adjacent water masses to cross over each other, the differential timing of sampling produces

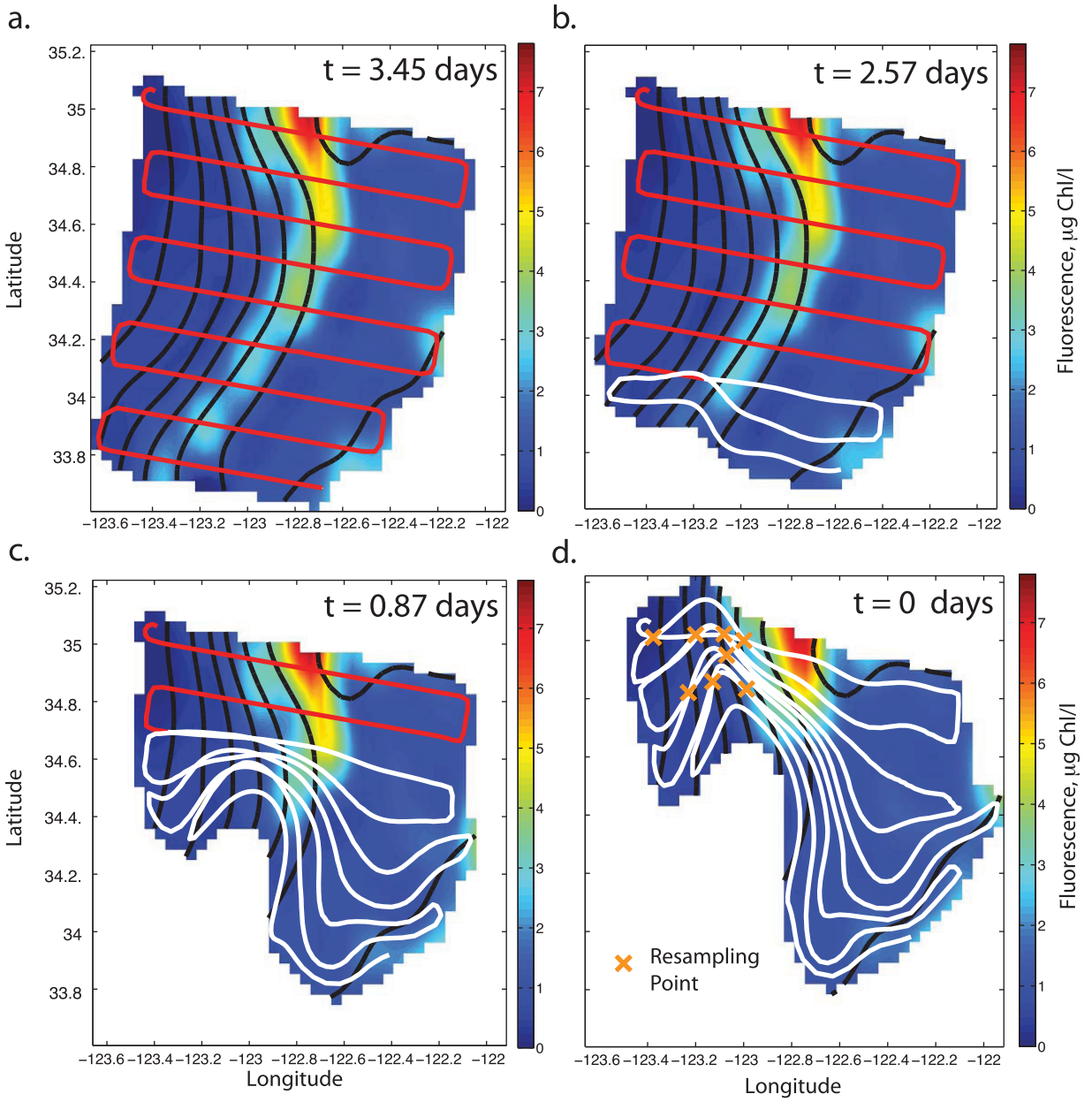

Figure 4. Sequential steps in the pseudo-Lagrangian transformation, showing objectively mapped Chl-a fluorescence with the initial survey distribution completed after (a) 3.45 days, moving back in time to (b) 2.57 days, (c) 0.87 day, and (d) 0 day after the survey began. Black lines are the streamlines; red line is the ship track; white line is the pseudo-Lagrangian remapped ship track moving backward in time. Figure 4d shows a pseudo-synoptic map of Chl-a fluorescence at the start of the survey. Note the enhanced spatial gradients of Chl-a fluorescence compared to Figure 4a. Orange crosses indicate water masses that were sampled twice during the survey.

regions where certain water positions are sampled twice (labeled as crosses in Figure 4d), or where a later sample reflects water "upstream" relative to an earlier sample. Our pseudo-Lagrangian transformation makes it possible to know what regions of sampling are (a) connected in a Lagrangian sense to each other through streamlines, and (b) whether or not samples acquired later in the survey actually represent samples that were downstream of samples acquired earlier in the survey.

Note that resampling of the same water parcel can only occur when the ship is moving in the direction of the flow; Survey 1 was made opposing the flow of the geostrophic jet, while Survey 2 was made in the direction of the jet. Therefore, resampling only occurs during Survey 2. Given our interest in estimating rates of change of a tracer (requiring multiple samples of the same water at different times), from now on we will focus on the high Chl-a feature located in the front during Survey 2.

The pseudo-Lagrangian map of the Chl-a fluorescence (Figure 4d) shows the distribution *given no local change in Chl-a fluorescence* during the survey. In regions where a water mass was sampled twice during the survey (i.e., the survey lines cross in the pseudo-Lagrangian map), we can make a direct comparison, thus creating some two-point time series to calculate the RHS of (1). For the majority of the survey region, however, Lagrangian resampling did not occur. Instead, a physical distance remains between the pseudo-Lagrangian-transformed water parcels, even though they share a trajectory. Given a stationary velocity field, the physical distance between two profiles that share a streamline amounts to a separation in time. From this perspective, $\mathbf{X}_2$ in Figure 3 comes from an earlier time in $\mathbf{X}_1$'s trajectory. We can use this information to calculate rates of change of the tracer along a streamline.

If the regions sampled twice have significantly different concentrations, then there must be temporal evolution of the tracer. The pseudo-Lagrangian distribution can thus be used to qualitatively gauge whether or not the RHS of (1) is different from zero. For the Chl-a fluorescence distribution (Figure 4d), the resampling points are unfortunately in regions of low fluorescence, and it is difficult to estimate net changes in Chl-a. The region of high Chl-a fluorescence near E-front shrinks in the along-front direction in the pseudo-Lagrangian transformation, indicating that these observations are both close together and part of a continuous Chl-a feature. Furthermore, the highest Chl-a observations seen in both Survey 1 and Survey 2 (Figure 2b) are found to the north, even though the surveys were done a month apart and in the opposite directions relative to the geostrophic flow. This result suggests a similar source of high Chl-a water, which can then be followed to calculate rates of change. The along-front decrease in Chl-a in the presence of an along-front flow implies that there must be a sink of Chl-a along the front. This observation of decreasing concentrations of Chl-a in cold filaments has been previously reported in the region [*Abbott et al.*, 1990; *Hood et al.*, 1991; *MacIsaac et al.*, 1985; *Jones et al.*, 1988; *Strub et al.*, 1991], supporting our contention that Chl-a is decreasing. Therefore, we are now in a position to use the velocity flow field to quantify the rates of change of our tracer.

4. Calculation of Net Rates of Change of Chl-a

To diagnose how the RHS of (1) evolves during a survey, we need to address the fact that few locations are sampled twice in pseudo-Lagrangian space. To accommodate this, we introduce a simple interpolation scheme to estimate the temporal changes in concentration. Subsequently, we explore sources of variability and error in the rate estimates.

4.1. Net Chl-a Growth Rate

Given the variability of biological processes, we want to maximize our use of observed data values at the location and time of collection. To do this, we start with the data locations $\mathbf{X}_{obs}$, i.e., the untransformed tracer field as it was sampled. Rather than integrating backward as in section 3, we move a water parcel $\mathbf{X}_\psi$ from the location and time of its initial observation $\mathbf{X}_{1obs}(x_1, y_1, t_{1obs})$ forward in time along its streamline. We advect $\mathbf{X}_\psi$ along its streamline for the amount of time it takes until we obtain the next observation along that same streamline, $\mathbf{X}_{2obs}(x_2, y_2, t_{2obs})$. Note that $\mathbf{X}_\psi$ may not have reached the location of $\mathbf{X}_{2obs}$ during this time (Figure 5).

To calculate a net rate, we need two Chl-a estimates from the same water parcel, and the time between samples. The time between samples for our rate measurement is the time elapsed between the two observations on the same streamline, namely $\Delta t = t_{2obs} - t_{1obs}$. For the initial Chl-a, we use the objectively mapped value at $\mathbf{X}_{1obs}$, which we call $C_1 = C(\mathbf{X}_{1obs})$. The final Chl-a value, C_2, is interpolated to the location $\mathbf{X}_\psi(x_\psi, y_\psi, t_{1obs}+\Delta t)$, otherwise known as $\mathbf{X}_\psi(x_\psi, y_\psi, t_{2obs})$. We now calculate a net specific growth rate, using the equation

$$r = \frac{1}{C_1[\mathbf{X}_1(x_1, y_1, t_{1obs})]} \cdot \frac{C_2[\mathbf{X}_\psi(x_\psi, y_\psi, t_{2obs})] - C_1[\mathbf{X}_1(x_1, y_1, t_{1obs})]}{\Delta t} \tag{10}$$

To estimate the rate of change of Chl-a fluorescence in the high-fluorescence feature seen at the front in the survey (Figure 4), we limit our present analyses to trajectories with initial fluorescence values ≥ 3 μg Chl-a L^{-1}. For Survey 2, this results in 156 independent estimates of the net specific growth rate (Figure 6). The calculations provide unusually high-resolution rate estimates over a large spatial region of $\sim$1200 km^2 (Figure 7), with a mean value of -0.167 day^{-1}. Given the overall decrease in observed Chl-a fluorescence along the geostrophic jet, the negative value of the mean net growth rate is not surprising. The utility of this analysis lies in the fact that what was previously a qualitative intuition (i.e., that Chl-a fluorescence decreased) has now been quantitatively estimated.

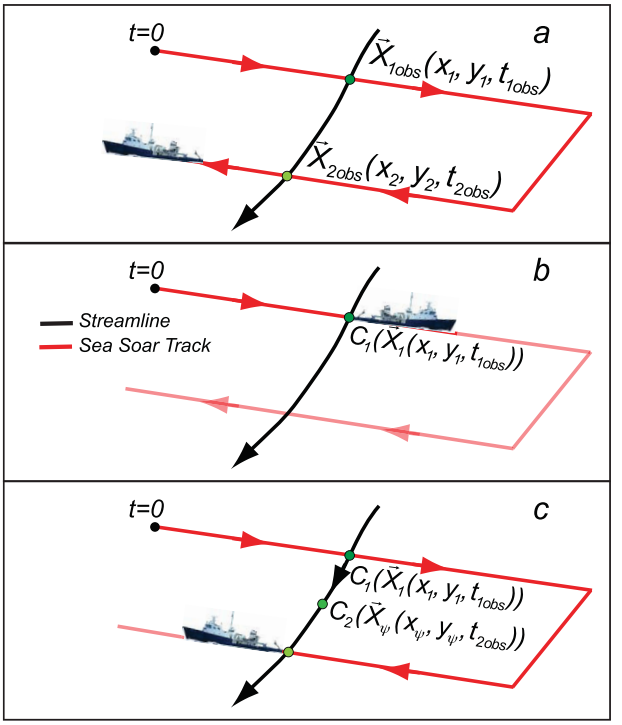

Figure 5. Rate calculation method. (a) Starting with two observations connected by a streamline, we forward advect the (b) first observation along its streamline until the ship collects the (c) second observation on the same streamline. The first water parcel's new position $\mathbf{X}_\psi$ is used with the objective map of tracer concentration to calculate the second concentration, C_2, for the rate measurement.

4.2. Error in the Rate Measurement

The previous section's calculation of net Chl-a growth rates is not very useful without some quantification of the error associated with the result. In order to achieve this, here we diagnose in (10) each source of error in turn. There are three pieces of information that are required to calculate r: the initial Chl-a, C_1, the final Chl-a, C_2, and the elapsed time Δt.

Since we chose the elapsed time to be based upon the times of our sampling locations, we do not assign an error to this term. The initial Chl-a value is determined from the relative error in the objective map, which has an assumed noise-to-signal ratio of $\leq$0.05. This value is indeed reflective of the proportion of the power spectrum selected with the 1 Hz smoothing and binning of the raw 24 Hz fluorescence time series. In using *Le Traon*'s [1990] method, anisotropic fluctuations to the assumed mean are added to the error due to the autocovariance of the tracer field in along and cross-front directions. We therefore get a standardized mean square error for each position in the tracer field, which is directly applied to the initial Chl-a value C_1.

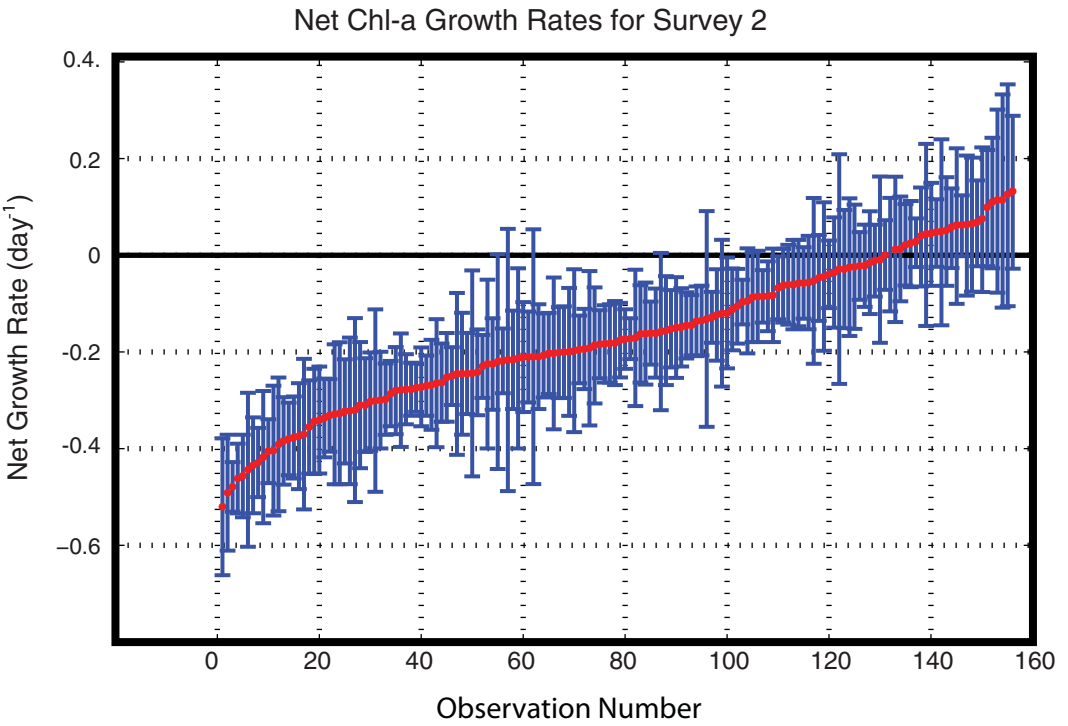

Figure 6. Calculated net Chl-a growth rates for Survey 2. Red dots indicate the rate estimate, and blue error bars are 95% confidence intervals as determined by equation (14).

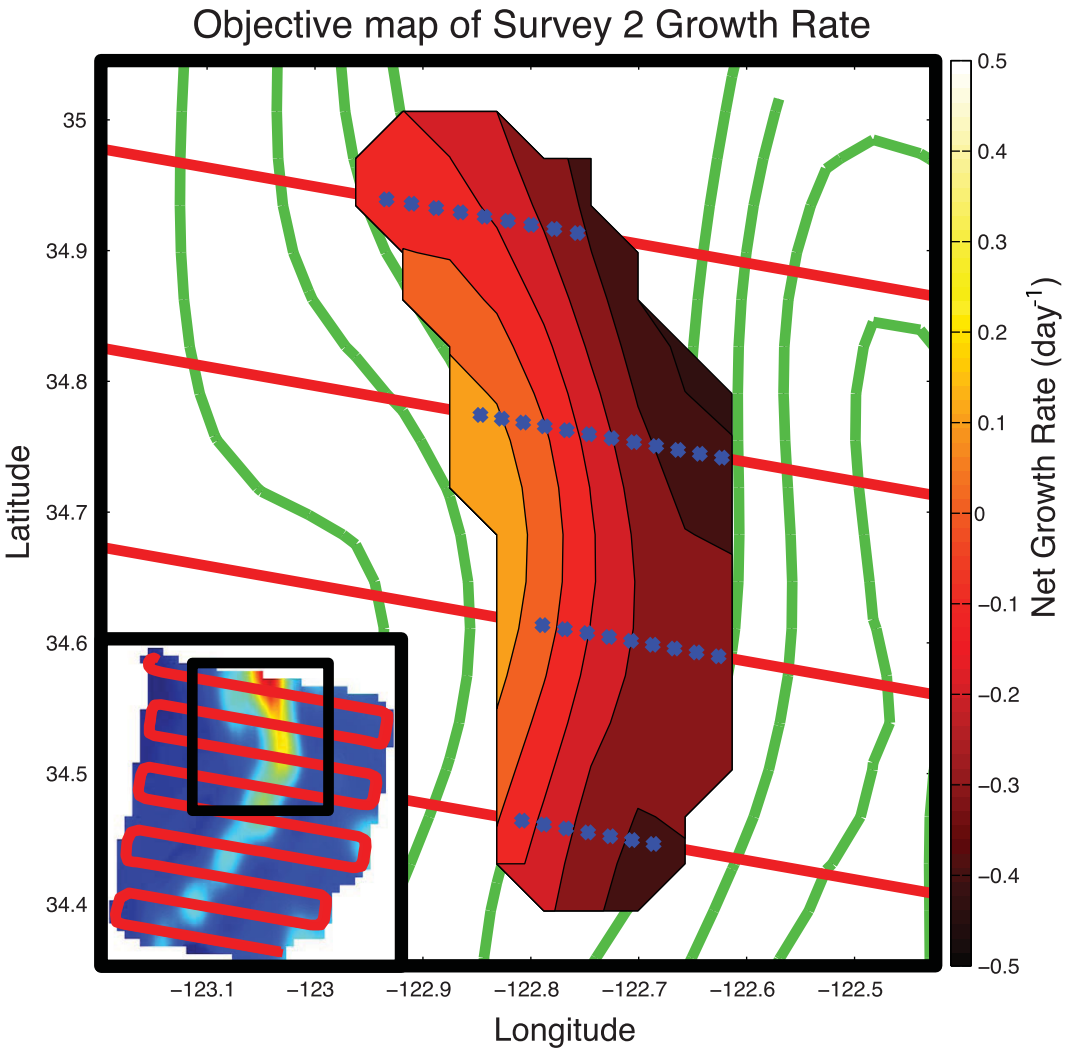

Figure 7. Objective map of estimated net growth rates at 27 m. Red line is the Survey 2 ship path. Green contours indicate Chl-a Fluorescence. Blue crosses indicate rate observation locations, totaling 37 at this depth. Inset is the survey path, with a black box indicating the zoomed-in region.

The final Chl-a value, C_2, will have not only the error assigned by the objective map, but also an error in the advection scheme in arriving at the correct position. To quantify this effect, we model the spatial misfit with a diffusion-like process. The validity in using a diffusion process to model misfit can be argued for by analyzing conservation of salinity. After conducting the pseudo-Lagrangian transformation from section 3 (and shown in Figure 4) on salinity, we use the difference between new mapped salinity and original salinity as a misfit metric. This difference is squared and summed over the map, then normalized by the number of observations. The time series of this misfit (not shown) grows over time in a qualitatively quadratic fashion, similar to particle dispersion at short time scales [*LaCasce*, 2008]. In the context of E-front, where salinity gradients should be mostly perpendicular to the geostrophic velocities, and salinity is assumed to be conserved, the misfits of salinity should correlate with misfits of position due to error in the velocity field. Therefore, a diffusion model is chosen in determining the velocity error.

A diffusion model requires a determination of the diffusivity, which we do by advecting salinity forward in time. For each rate measurement, there is an associated salinity difference between the observations connected by streamlines. The time T necessary for advection is known. The relevant distance scale, L, is determined moving along the survey line and subsequently identifying the position that matches the original salinity. The apparent diffusivity, κ, can be found by the following relation:

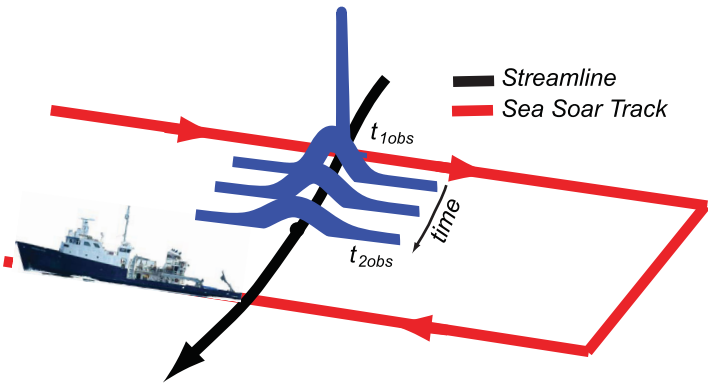

Figure 8. Diffusion-like model used for rate measurement error. The location probability distribution begins as a delta function at t_{1obs}, and sequentially spreads according to equation (12) until t_{2obs}.

$$\kappa = \frac{L^2}{4T} \tag{11}$$

The estimates of κ arrived at by advection of salinity has a fat-tailed distribution, and we choose the median value of 120 m^2/s to represent the velocity misfit.

Taking the observation C_1 at the point $\mathbf{X}_{1obs}$ as a discrete point whose position is known with certainty, we represent the probability distribution of its initial location as the Dirac delta function. This distribution has many useful properties, including the fact that its integral over all space is one, making it appropriate to use as a pdf. Using the Dirac delta function as the initial condition at $\mathbf{X}_{1obs}$, the subsequent probability distribution of position as a function of time Δt is

$$\Phi(x, \Delta t) = \frac{1}{\sqrt{4\pi\kappa\Delta t}} \exp\left(-\frac{x^2}{4\kappa\Delta t}\right) \tag{12}$$

Equation (12) gives the probability distribution for the cross-streamline location of a water parcel starting at $\mathbf{X}_{1obs}$ that is advecting along a streamline assuming a velocity error modeled by diffusion. Given the elapsed time Δt, one can calculate a probability density function for positions on either side of the water parcel centered at $\mathbf{X}_{1obs}$ (Figure 8), and we here select the distances corresponding to 95% confidence intervals.

Inclusion of the diffusion-like model produces two displacements representative of velocity error. Evaluating Chl-a at these two locations, their relative difference from C_2 produces a similar 95% confidence interval in the variability of C_2. Normally, the error from the objective map would be included in the range of these Chl-a values, but in practice for our application, the modeled diffusion variance was an order of magnitude larger than the objective map's, and so the objective map error is ignored for C_2.

Armed with the variances for both C_1 and C_2, we now return to the rate calculation. Multiplying (10) by Δt, which we assume to be known, and splitting the numerator, we arrive at

$$r\Delta t = \frac{C_2}{C_1} - \frac{C_1}{C_1} \Rightarrow r\Delta t = \frac{C_2}{C_1} - 1 \tag{13}$$

Through this manipulation, the only portion with error is the ratio C_2/C_1, since by definition C_1/C_1 will be equal to 1. The probability distribution for ratios of Gaussian variables is provided by *Hinkley* [1969] and becomes

$$P(z) = \frac{b(z)d(z)}{\sqrt{2\pi}\sigma_2\sigma_1 a^3(z)}\left[\Lambda\left\{\frac{b(z)}{\sqrt{1-\rho^2}a(z)}\right\} - \Lambda\left\{-\frac{b(z)}{\sqrt{1-\rho^2}a(z)}\right\}\right] + \frac{\sqrt{1-\rho^2}}{\pi\sigma_2\sigma_1 a^2(z)}\exp\left\{-\frac{c}{2(1-\rho^2)}\right\} \tag{14}$$

with z being C_2/C_1, standard errors σ_1,σ_2, means μ_1, μ_2, and correlation ρ, with the definitions

$$a(z)=\left(\frac{z^2}{{\sigma_2}^2}-\frac{2\rho z}{\sigma_2\sigma_1}+\frac{1}{\sigma_1^2}\right)^{\frac{1}{2}} \tag{15}$$

$$b(z)=\frac{\mu_2 z}{{\sigma_2}^2}-\frac{\rho(\mu_2+\mu_1 z)}{\sigma_2\sigma_1}+\frac{\mu_1}{\sigma_1^2} \tag{16}$$

$$c=\frac{{\mu_2}^2}{{\sigma_2}^2}-\frac{2\rho\mu_2\mu_1}{\sigma_2\sigma_1}+\frac{{\mu_1}^2}{\sigma_1^2} \tag{17}$$

$$d(z)=\exp\left\{\frac{b^2(z)-ca^2(z)}{2(1-\rho^2)a^2(z)}\right\} \tag{18}$$

$$\Lambda(y)=\int_{-\infty}^{y}\phi(u)du,\ \text{ where }\ \phi(u)=\frac{1}{\sqrt{2\pi}}\exp\left\{-\frac{1}{2}u^2\right\} \tag{19}$$

The standard error and means change with each rate measurement, and the correlation was found for the 156 measurements to be 0.91. With the ratio pdf calculated, we finally arrive at the ability to find 95% confidence intervals for our ratio measurements. Taking these values, subtracting one and multiplying by the observation's Δt gets the confidence interval for each rate, which we display in Figure 6, with the rates presented in increasing order for visual comparison. Out of 156 points, 64% are found to be significantly less than zero, with none found to be significantly greater than zero.

Through the adoption of a diffusion-like model to account for error in the velocity field, it is thus possible to quantify to what extent the pseudo-Lagrangian method produces meaningful rates for a given application.

4.3. Comparison to Traditional Rate Measurements

The pseudo-Lagrangian approach to estimating net rates from tracer data will be a valuable tool in evaluating tracer evolution in conjunction with other, more traditional methods. Since measured tracer concentration reflects all the processes that occur in a water parcel, the net rates derived from our described method provide a rate ostensibly comparable with a total budget of rate measurements based on individual mechanisms. Examples of traditional rate measurements affecting phytoplankton include: dilution experiments to quantify phytoplankton growth and microzooplankton grazing [*Landry and Hassett*, 1982], mesozooplankton gut fluorescence data to determine mesozooplankton grazing [*Mackas and Bohrer*, 1976; *Kiørboe et al*., 1985], and sediment traps to estimate vertical flux of particulates [*Knauer et al*., 1979]. Apart from the growth measured in dilution experiments, most of these observations quantify loss terms in the RHS of (1). Therefore, rate estimates from any of these traditional methods, which inevitably leave out some loss processes, should be slightly more positive than the rate found by the pseudo-Lagrangian method, which implicitly includes them all.

Additionally, careful attention must be paid to confounding effects of these individual rate measurements. For example, the bottle incubations used in dilution experiments exclude mesozooplankton grazers, and so the estimated net growth rate includes a possible predation release from mesozooplankton. Further problems arise comparing biological data from localized water parcels to data reflecting integrated quantities, for example, comparing bottle dilution rates with vertical plankton tows for mesozooplankton grazing. While these different methods lead to biological rates of similar units (e.g., day^{-1}), it is impossible to assume a priori that these rates should be comparable such that they can be linearly added and subtracted to match up to a total net rate as calculated in the pseudo-Lagrangian method.

In our present use of the pseudo-Lagrangian technique, we use an ensemble approach wherein all observations of sufficient Chl-a are used to estimate net changes of tracer concentration. Therefore, values from various depths but belonging to the same high Chl-a feature are used. In this case, vertically integrated rate measurements, such as mesozooplankton gut fluorescence tows, should be comparable with the pseudo-Lagrangian rate, assuming that grazing can be equally applied across the feature. Localized measurements, such as dilution rates, should be compared with pseudo-Lagrangian rates measured from observations at the same depth. Calculating the relative variance of net growth rates from both constant-depth and integrated perspectives can provide an avenue to account for the bias of methodology in traditional rate measurements.

Due to the experimental layout of the E-Front cruise, the only experimental rate estimates that were spatiotemporally close to the second SeaSoar survey were the mesozooplankton gut fluorescence data. These data were collected and processed as described in *Landry et al*. [2009]. The mesozooplankton grazing rate for our feature averages to -0.3 day^{-1} (M. D. Ohman, personal communication, 2015). These values compare well with some of the pseudo-Lagrangian observations, though the majority are significantly more positive than -0.3 (56%). While strong grazing provides a mechanism for the overall decrease in Chl-a, the magnitude suggests that some positive contribution to the RHS of (1) is present, such as in situ growth of Chl-a. A rigorous and quantitative comparison of pseudo-Lagrangian and experimentally derived rates, however, is beyond the scope of this study.

5. Discussion

The methods outlined above provide two results: (1) a transformed pseudo-Lagrangian map of sampled data that reflects more accurate relative positioning of samples obtained in a moving fluid, and (2) a distribution of estimated rates of change of tracer concentration to quantify the RHS of (1). The most significant assumption necessary in our analysis is the presence of a stationary, geostrophic velocity field. We quantified the possible contribution of ageostrophic vertical upwelling or subduction through the omega equation and determined that it was small enough to ignore for our present analysis. However, incorporating these effects with others, such as wind forcing or Stokes drift, would help to assess their contribution to the observed decrease in Chl-a. Without direct measurements, some of these effects are difficult to incorporate into our velocity field in a consistent manner. Progress is being made on understanding the impact of these phenomena upon ocean fronts [*McWilliams and Fox-Kemper*, 2013], and we plan to address this issue in the future. Given these dynamical omissions, our present use of the geostrophic velocity field still yields useful insights.

The pseudo-Lagrangian transformation allows for a better interpretation of a given sampling distribution, and is a useful way to reorganize survey locations into a single, consistent snapshot (Figure 4d). Without the transformation, we would not know the extent of resampling that occurred in the western portion of Survey 2. Generally speaking, this remapping of the survey conducted in the direction of the dominant flow produces regions that allow point-to-point comparisons for quantifying the RHS of (1). Unfortunately, in our data set, this was not possible due to the very low Chl-a concentration there. We also used the pseudo-Lagrangian map to interpret whether the Chl-a concentrations were static over time. A differencing of the transformed map with the original distribution, though of possible use qualitatively, cannot be used directly for rate estimates due to the overlapping of measurements from different times. We therefore use our forward-advecting methodology to estimate rates.

The application of our rate estimation methodology to E-Front yields spatially resolved rates of change of our chosen tracer, Chl-a fluorescence. What is at first visually obvious from Figure 2d—a general decrease in Chl-a along the front—has now been quantitatively estimated from ensemble observations. The usual field methods for estimating such rates (e.g., in situ dilution methods or primary productivity measurements) require first identifying the feature, returning to it, and incubating experimental flasks on a platform that follows the flow. The result is a single point measurement, obtained through a great deal of effort both on the ship and subsequently in the lab. By selectively choosing our Chl-a threshold and focusing on the high-fluorescence region, we obtained 156 estimates of net growth rate within this feature. Together, these estimates yield a range of rates comparable to those estimated from gut fluorescence, and well within the range of rates observed in other studies of our region [*Landry et al*., 2009; *Li et al*., 2010, 2011].

One practical consequence of our analyses is that the survey direction relative to the flow matters. As previously mentioned, sampling in the direction of the geostrophic jet allows for identification of resampled water parcels. Though these regions were not used in our analysis, the fact remains that resampling of water parcels would not occur in a survey conducted upstream, where all later observations would always come from water parcels located farther upstream. Thus, in light of the pseudo-Lagrangian transformation, planning a ship track designed for biogeochemical tracer rate analysis would dictate a downstream sampling strategy.

Another consequence of sampling direction is the sharpening and weakening of observed tracer gradients. *Rixen et al*. [2001] note this in their numerical study replicating asynoptic data collection: upstream

(downstream) sampling sharpens (weakens) estimated tracer gradients. For our rate measurements, this would imply that our results from Survey 2, conducted downstream, underestimate the true gradients in Chl-a (as is clear from the pseudo-Lagrangian remapped data, Figure 4), and hence produce reduced magnitudes of the net growth rate. Our conclusion of a nonzero rate of change is thus conservative. *Rixen et al*. [2001] pursued an approach whereby dynamically active tracers (temperature, salinity, and density) were advected and used in a new calculation of geostrophic velocity and tracer fields. This was done iteratively until convergence was reached. While this approach is useful for creating a self-consistent density and geostrophic velocity field, there is no equivalent way to sequentially alter and correct data from biogeochemical tracers, which do not impact the physical dynamics.

Throughout this study, we have made reference to calculating net tracer growth rates. This nomenclature requires some clarification. First, our use of Chl-a fluorescence means that the calculated rates are exactly that: the rate of change of Chl-a. Chlorophyll is not directly useful in quantifying phytoplankton biomass or carbon [*Kruskopf and Flynn*, 2006], and so the change in chlorophyll does not translate into a change in the population or organic carbon per se. However, many of the rate measurements mentioned in section 4.3 measure chlorophyll, and so measureable ecological rates, such as grazing, can be expressed as the rate of removal of Chl-a. The ability to compare this methodology with other traditional methods by using the same tracer is of primary importance; if one wishes to express changes in biomass or carbon, then direct measurements are necessary. Second, the word "net" in net tracer growth reflects how this method measures the change due to all the biological processes on the RHS of (1) acting at once, i.e., growth, grazing, sinking, swimming, etc. Other in situ measurements of rates isolate and resolve only certain ecosystem processes. As a result, our method produces a quantitative rate budget constraint that must be satisfied when compared to all other ecosystem processes affecting Chl-a.

Looking at the spatial map of net growth rates as determined by advection only (Figure 7), there are visible gradients in the rate measurements, with rates located in the western part of the feature having higher absolute values than those to the east. If the high Chl-a feature was indeed evolving as a whole, one might expect zero spatial gradient. This gradient may arise from errors in our geostrophic velocities following the true trajectory of the feature, where values near the edge may erroneously wander in and out of the distribution. There is no immediate way to remedy this situation, apart from including more complicated and accurate physical processes. Regardless, the range of rate values found in our spatial map are reasonable and the possible variability due to advective error equivalent to other in situ observations [*Landry et al*., 2009; *Li et al*., 2010, 2011].

6. Conclusions

The pseudo-Lagrangian approach described here provides a powerful tool for analyzing biogeochemical tracer fields from spatial surveys. Though the notion of utilizing Eulerian velocity fields to advect Lagrangian positions is not novel, here we take advantage of what is usually considered a limitation: the nonsynopticity of ship sampling. A ship can be only in one place at one time, while the fluid is simultaneously moving, and advecting tracers with it. Thus, ship surveys always alias the spatial distributions of properties. Here in a situation where the physical dynamics can be considered quasi-stationary, we utilize these time-aliased observations to systematically produce estimates of short-term tracer dynamics.

The tracer transformation in section 3 allows for reanalysis of observations to determine whether the RHS of (1) is nonzero, that is, whether there are local rates of change of the tracer not driven by advection. In phytoplankton communities where large rates of growth and mortality often cancel to create a near balance of the RHS of (1), determining its sign and difference from zero is often nontrivial [*Jickells et al*., 2008]. By removing the effects of advection, an investigator can now determine whether certain observations are replicates of the same water parcel, and where temporally distinct observations originated relative to each other in space.

The applicability of the pseudo-Lagrangian transformation requires satisfying several conditions. In regions where high-frequency water movements dominate local flow and create essentially stochastic noise overlying a weaker mean circulation, such as nearshore coastal regions, the lack of deterministic knowledge of the flow field makes pseudo-Lagrangian advection impossible to implement. Considering the size and speed of research vessels, the physical features most amenable to pseudo-Lagrangian analyses would be

mesoscale regions, such as fronts and eddies, that are largely in geostrophic balance and are relatively stationary during the survey period.

A further limitation of the method is that the biogeochemical tracers of interest must be able to be rapidly sensed by a towed platform to create the objectively mapped field. For example, the SeaSoar deployment in this study contained a fluorometer, transmissometer, and oxygen sensor. While some measurements can be used as proxies for other desired variables (such as dissolved oxygen in calculating aragonite saturation) [*Alin et al*., 2012; *Bednaršek and Ohman*, 2015], other quantities still require intense sampling and possible postprocessing in the lab. Recent development of remote sensing equipment for difficult biogeochemical measurements such as pH [*Martz et al*., 2010] and alkalinity [*Spaulding et al*., 2014] will allow for their eventual inclusion in more ambitious deployments. Currently, large-scale programs, such as Argo [*Freeland et al*., 2010], are driving instrument development toward autonomous and low-power miniaturized devices. Towed instruments do not have such a power limitation, providing a deployment platform for new instruments before they are optimized for autonomous vehicles. Data acquired by these new technologies on platforms such as SeaSoar could benefit from the methodology outlined here to provide spatially resolved rate estimates not currently available.

The tracer rate analysis method presented here also allows for quantifying the dynamics underlying observed tracer distributions. Still, the analyses must be carefully interpreted. First, the limitations of a given tracer must be recognized. Though Chl-a fluorescence is often used as a proxy for phytoplankton biomass, we strictly discourage interpreting our Chl-a net growth rates as a change in biomass or carbon, and limit conclusions to factors directly affecting Chl-a. Additionally, the separate terms on the RHS of (1) cannot be distinguished from each other using our technique: we obtain a *net* rate resulting from all the possible processes in (1). The *net* rate calculated from these in situ observations complement the traditional, difficult biogeochemical rate measurements that can separate the various processes on the RHS of (1) (e.g., growth and grazing rate measurements, sinking fluxes from sediment traps, etc.) by providing estimates for the overall rate balance.

In conclusion, our pseudo-Lagrangian scheme provides a method to remap observational data to remove aliasing due to advection, and produces high-resolution estimates of net rates over spatial scales that are not achievable using traditional methods of direct observation. The limitations of the pseudo-Lagrangian method arise mainly from undetermined physical flows, and the suite of tracers available for towed deployment. Extension of the technique's applicability is possible through advances in instrument development. Used as a complementary data set to more traditional analyses at sea, the pseudo-Lagrangian technique provides a large set of independent observations to compare with the usual syntheses of disparate measurements used to calculate ecological and biogeochemical budgets.

Acknowledgments

The data for this paper are available upon request from the National Science Foundation California Current Ecosystem (CCE) Long Term Ecological Research (LTER) site (http://cce.lternet.edu/). This work was supported by National Science Foundation (NSF) funding (1026607) for the CCE-LTER site. A.D. would like to acknowledge private funding support from Jeffrey Bohn. We are grateful to the captain and crew of the R/V Melville and all the participants of CCE-LTER August 2012 process cruise. In particular, we thank Carl Matson for SeaSoar deployment and recovery, Alexander Chekalyuk and Mark Hafez for ALF-A data, along with Ralf Goericke for Chlorophyll data. The manuscript benefitted greatly from the input of Mark Ohman, Michael Landry, and two anonymous reviewers.

References

Abbott, M. R., and P. M. Zion (1985), Satellite observations of phytoplankton variability during an upwelling event, *Cont. Shelf Res.*, *4*(6), 661–680, doi:10.1016/0278-4343(85)90035-4.

Abbott, M. R., K. H. Brink, C. R. Booth, D. Blasco, L. A. Codispoti, P. P. Niiler, and S. R. Ramp (1990), Observations of phytoplankton and nutrients from a Lagrangian drifter off northern California, *J. Geophys. Res.*, *95*(C6), 9393–9409, doi:10.1029/JC095iC06p09393.

Alin, S. R., R. A. Feely, A. G. Dickson, J. M. Hernández-Ayón, L. W. Juranek, M. D. Ohman, and R. Goericke (2012), Robust empirical relationships for estimating the carbonate system in the southern California Current System and application to CalCOFI hydrographic cruise data (2005–2011), *J. Geophys. Res.*, *117*, C05033, doi:10.1029/2011JC007511.

Allen, J. T., D. A. Smeed, A. J. G. Nurser, J. W. Zhang, and M. Rixen (2001), Diagnosis of vertical velocities with the QG omega equation: An examination of the errors due to sampling strategy, *Deep Sea Res., Part I*, *48*(2), 315–346, doi:10.1016/s0967-0637(00)00035-2.

Andrews, D. G., and M. E. McIntyre (1978), An exact theory of nonlinear waves on a Lagrangian-mean flow, *J. Fluid Mech.*, *89*(4), 609–646, doi:10.1017/s0022112078002773.

Bednaršek, N., and M. D. Ohman (2015), Changes in pteropod distributions and shell dissolution across a frontal system in the California Current System, *Mar. Ecol. Prog. Ser.*, *523*, 93–103, doi:10.3354/meps11199.

Blanke, B., and S. Raynaud (1997), Kinematics of the Pacific Equatorial Undercurrent: An Eulerian and Lagrangian approach from GCM results, *J. Phys. Oceanogr.*, *27*(6), 1038–1053, doi:10.1175/1520-0485(1997)027<1038:KOTPEU>2.0.CO;2.

Bowman, K. P., J. C. Lin, A. Stohl, R. Draxler, P. Konopka, A. Andrews, and D. Brunner (2013), Input data requirements for Lagrangian trajectory models, *Bull. Am. Meteorol. Soc.*, *94*(7), 1051–1058, doi:10.1175/BAMS-D-12-00076.

Boyd, P. W., et al. (2007), Mesoscale iron enrichment experiments 1993–2005: Synthesis and future directions, *Science*, *315*(5812), 612–617, doi:10.1126/science.1131669.

Bracco, A., A. Provenzale, and I. Scheuring (2000), Mesoscale vortices and the paradox of the plankton, *Proc. R. Soc. London, Ser. B*, *267*(1454), 1795–1800, doi:10.1098/rspb.2000.1212.

Chekalyuk, A. M., and M. A. Hafez (2008), Advanced laser fluorometry of natural aquatic environments, *Limnol. Oceanogr. Methods*, *6*, 591–609, doi:10.4319/lom.2008.6.591.

Chekalyuk, A. M., and M. A. Hafez (2011), Photo-physiological variability in phytoplankton chlorophyll fluorescence and assessment of chlorophyll concentration, *Optics Express*, *19*(23), 22,643–22,658, doi:10.1364/OE.19.022643.

D'Asaro, E. A. (2003), Performance of autonomous Lagrangian floats, *J. Atmos. Oceanic Technol.*, *20*(6), 896–911, doi:10.1175/1520-0426(2003)020<0896:POALF>2.0.CO;2.

D'Asaro, E. A., C. Lee, L. Rainville, R. Harcourt, and L. Thomas (2011), Enhanced turbulence and energy dissipation at ocean fronts, *Science*, *332*(6027), 318–322, doi:10.1126/science.1201515.

Doglioli, A. M., M. Veneziani, B. Blanke, S. Speich, and A. Griffa (2006), A Lagrangian analysis of the Indian-Atlantic interocean exchange in a regional model, *Geophys. Res. Lett.*, *33*, L14611, doi:10.1029/2006GL026498.

Doglioli, A. M., F. Nencioli, A. A. Petrenko, G. Rougier, J. L. Fuda, and N. Grima (2013), A software package and hardware tools for in situ experiments in a Lagrangian reference frame, *J. Atmos. Oceanic Technol.*, *30*(8), 1940–1950, doi:10.1175/JTECH-D-12-00183.1.

d'Ovidio, F., V. Fernández, E. Hernández-García, and C. López (2004), Mixing structures in the Mediterranean Sea from finite-size Lyapunov exponents, *Geophys. Res. Lett.*, *31*, L17203, doi:10.1029/2004GL020328.

d'Ovidio, F., S. De Monte, S. Alvain, Y. Dandonneau, and M. Lévy (2010), Fluid dynamical niches of phytoplankton types, *Proc. Natl. Acad. Sci. U. S. A.*, *107*(43), 18,366–18,370, doi:10.1073/pnas.1004620107.

Dragani, R., G. Redaelli, G. Visconti, A. Mariotti, V. Rudakov, A. R. Mackenzie, and L. Stefanutti (2002), High-resolution stratospheric tracer fields reconstructed with Lagrangian techniques: A comparative analysis of predictive skill, *J. Atmos. Sci.*, *59*(12), 1943–1958, doi:10.1175/1520-0469(2002)059<1943:HRSTFR>2.0.CO;2.

Firing, E., and J. M. Hummon (2010), Shipboard ADCP measurements, in *The GO-SHIP Repeat Hydrography Manual: A Collection of Expert Reports and Guidelines. IOCCP Rep.* 14, ICPO Publication Series Number 134. [Available at http://www.go-ship.org/HydroMan.html.]

Freeland, H. J., et al. (2010), Argo – A Decade of Progress, in *OceanObs'09: Sustained Ocean Observations and Information for Society, vol. 2*, Venice, Italy, 2125 September 2009, edited by J. Hall, D. E. Harrison, and D. Stammer, ESA Publication WPP-306, doi:10.5270/oceanobs09.cwp.32.

Gurvich, A. S., and A. M. Yaglom (1967), Breakdown of eddies and probability distributions for small-scale turbulence, *Phys. Fluids*, *10*(9), S59–S65, doi:10.1063/1.1762505.

Hinkley, D. V. (1969), On the ratio of two correlated normal random variables, *Biometrika*, *56*(3), 635–639, doi:10.1093/biomet/56.3.635.

Hood, R. R., M. R. Abbott, and A. Huyer (1991), Phytoplankton and photosynthetic light response in the coastal transition zone off northern California in June 1987, *J. Geophys. Res.*, *96*(C8), 14,769–14,780, doi:10.1029/91JC01208.

Hoskins, B. J., I. Draghici, and H. C. Davies (1978), A new look at the ω-equation, *Q. J. R. Meteorol. Soc.*, *104*(439), 31–38, doi:10.1256/smsqj.43902.

Jickells, T. D., et al. (2008), A Lagrangian biogeochemical study of an eddy in the Northeast Atlantic, *Prog. Oceanogr.*, *76*(3), 366–398, doi:10.1016/j.pocean.2008.01.006.

Jones, B. H., L. P. Atkinson, D. Blasco, K. H. Brink, and S. L. Smith (1988), The asymmetric distribution of chlorophyll associated with a coastal upwelling center, *Cont. Shelf Res.*, *8*(10), 1155–1170, doi:10.1016/0278-4343(88)90017-9.

Kiørboe, T., F. Møhlenberg, and H. U. Riisgård (1985), In situ feeding rates of planktonic copepods: A comparison of four methods, *J. Exp. Mar. Biol. Ecol.*, *88*, 67–81, doi:10.1016/0022-0981(85)90202-3.

Knauer, G. A., J. H. Martin, and K. W. Bruland (1979), Fluxes of particulate carbon, nitrogen, and phosphorus in the upper water column of the northeast Pacific, *Deep Sea Res., Part A*, *26*(1), 97–108, doi:10.1016/0198-0149(79)90089-X.

Kolmogorov, A. N. (1962), A refinement of previous hypotheses concerning the local structure of turbulence in a viscous incompressible fluid at high Reynolds number, *J. Fluid Mech.*, *13*(1), 82–85, doi:10.1017/S0022112062000518.

Koszalka, I., A. Bracco, C. Pasquero, and A. Provenzale (2007), Plankton cycles disguised by turbulent advection, *Theor. Popul. Biol.*, *72*(1), 1–6, doi:10.1016/j.tpb.2007.03.007.

Krause, G. H., and E. Weis (1991), Chlorophyll fluorescence and photosynthesis: The basics, *Annu. Rev. Plant Biol.*, *42*(1), 313–349, doi:10.1146/annurev.pp.42.060191.001525.

Kruskopf, M., and K. J. Flynn (2006), Chlorophyll content and fluorescence responses cannot be used to gauge reliably phytoplankton biomass, nutrient status or growth rate, *New Phytol.*, *169*(3), 525–536, doi:10.1111/j.1469-8137.2005.01601.x.

Kunze, E., and T. B. Sanford (1984), Observations of near-inertial waves in a front, *J. Phys. Oceanogr.*, *14*(3), 566–581, doi:10.1175/1520-0485(1984)014<0566:OONIWI>2.0.CO;2.

LaCasce, J. H. (2008), Statistics from Lagrangian observations, *Prog. Oceanogr.*, *77*(1), 1–29, doi:10.1016/j.pocean.2008.02.002.

Landry, M. R., and R. P. Hassett (1982), Estimating the grazing impact of marine micro-zooplankton, *Mar. Biol.*, *67*, 283–288, doi:10.1007/BF00397668.

Landry, M. R., M. D. Ohman, R. Goericke, M. R. Stukel, and K. Tsyrklevich (2009), Lagrangian studies of phytoplankton growth and grazing relationships in a coastal upwelling ecosystem off Southern California, *Prog. Oceanogr.*, *83*(1), 208–216, doi:10.1016/j.pocean.2009.07.026.

Law, C. S., A. J. Watson, M. I. Liddicoat, and T. Stanton (1998), Sulphur hexafluoride as a tracer of biogeochemical and physical processes in an open-ocean iron fertilisation experiment, *Deep Sea Res. Part II*, *45*(6), 977–994, doi:10.1016/s0967-0645(98)00022-8.

Le Traon, P. Y. (1990), A method for optimal analysis of fields with spatially variable mean, *J. Geophys. Res.*, *95*(C8), 13,543–13,547, doi:10.1029/JC095iC08p13543.

Lehahn, Y., F. d'Ovidio, M. Lévy, and E. Heifetz (2007), Stirring of the northeast Atlantic spring bloom: A Lagrangian analysis based on multisatellite data, *J. Geophys. Res.*, *112*, C08005, doi:10.1029/2006JC003927.

Lett, C., P. Verley, C. Mullon, C. Parada, T. Brochier, P. Penven, and B. Blanke (2008), A Lagrangian tool for modelling ichthyoplankton dynamics, *Environ. Modell. Software*, *23*(9), 1210–1214, doi:10.1016/j.envsoft.2008.02.005.

Li, Q. P., D. A. Hansell, D. J. McGillicuddy, N. R. Bates, and R. J. Johnson (2008), Tracer-based assessment of the origin and biogeochemical transformation of a cyclonic eddy in the Sargasso Sea, *J. Geophys. Res.*, *113*, C10006, doi:10.1029/2008JC004840.

Li, Q. P., P. J. S. Franks, M. R. Landry, R. Goericke, and A. G. Taylor (2010), Modeling phytoplankton growth rates and chlorophyll to carbon ratios in California coastal and pelagic ecosystems, *J. Geophys. Res.*, *115*, G04003, doi:10.1029/2009JG001111.

Li, Q. P., P. J. S. Franks, and M. R. Landry (2011), Microzooplankton grazing dynamics: Parameterizing grazing models with dilution experiment data from the California Current Ecosystem, *Mar. Ecol. Prog. Ser.*, *438*, 59–69, doi:10.3354/meps09320.

Lueck, R. G., and J. J. Picklo (1990), Thermal inertia of conductivity cells: Observations with a Sea-Bird cell, *J. Atmos. Oceanic Technol.*, *7*(5), 756–768, doi:10.1175/1520-0426(1990)007<0756:TIOCCO>2.0.CO;2.

MacIsaac, J. J., R. C. Dugdale, R. T. Barber, D. Blasco, and T. T. Packard (1985), Primary production cycle in an upwelling center, *Deep Sea Res., Part A*, *32*(5), 503–529, doi:10.1016/0198-0149(85)90042-1.

Mackas, D., and R. Bohrer (1976), Fluorescence analysis of zooplankton gut contents and an investigation of diel feeding patterns, *J. Exp. Mar. Biol. Ecol.*, *25*, 77–85, doi:10.1016/0022-0981(76)90077-0.

Martin, A. P. (2003), Phytoplankton patchiness: The role of lateral stirring and mixing, *Prog. Oceanogr.*, *57*(2), 125–174, doi:10.1016/s0079-6611(03)00085-5.

Martz, T. R., J. G. Connery, and K. S. Johnson (2010), Testing the Honeywell Durafet® for seawater pH applications, *Limnol. Oceanogr. Methods*, *8*, 172–184, doi:10.4319/lom.2010.8.172.

McWilliams, J. C., and B. Fox-Kemper (2013), Oceanic wave-balanced surface fronts and filaments, *J. Fluid Mech.*, *730*, 464–490, doi:10.1017/jfm.2013.348.

Methven, J., S. R. Arnold, F. M. O'Connor, H. Barjat, K. Dewey, J. Kent, and N. Brough (2003), Estimating photochemically produced ozone throughout a domain using flight data and a Lagrangian model, *J. Geophys. Res.*, *108*(D9), 4271, doi:10.1029/2002JD002955.

Molcard, A., L. I. Piterbarg, A. Griffa, T. M. Özgökmen, and A. J. Mariano (2003), Assimilation of drifter observations for the reconstruction of the Eulerian circulation field, *J. Geophys. Res.*, *108*(C3), 3056, doi:10.1029/2001JC001240.

Müller, P., X. P. Li, and K. K. Niyogi (2001), Non-photochemical quenching: A response to excess light energy, *Plant Physiol.*, *125*(4), 1558–1566, doi:10.1104/pp.125.4.1558.

Nilsson, E. D., and C. Leck (2002), A pseudo-Lagrangian study of the sulfur budget in the remote Arctic marine boundary layer, *Tellus, Ser. B*, *54*(3), 213–230, doi:10.3402/tellusb.v54i3.16662.

Pallàs-Sanz, E., T. M. S. Johnston, and D. L. Rudnick (2010), Frontal dynamics in a California Current System shallow front: 1. Frontal processes and tracer structure, *J. Geophys. Res.*, *115*, C12067, doi:10.1029/2009JC006032.

Powell, T. M., and A. Okubo (1994), Turbulence, diffusion and patchiness in the sea, *Philos. Trans. R. Soc. London B*, *343*(1303), 11–18, doi:10.1098/rstb.1994.0002.

Rixen, M., J. M. Beckers, and J. T. Allen (2001), Diagnosis of vertical velocities with the QG Omega equation: A relocation method to obtain pseudo-synoptic data sets, *Deep Sea Res., Part I*, *48*(6), 1347–1373, doi:10.1016/S0967-0637(00)00085-6.

Rixen, M., et al. (2003), Along or across front survey strategy? An operational example at an unstable front, *Geophys. Res. Lett.*, *30*(1), 1017, doi:10.1029/2002GL015341.

Rudnick, D. L. (1996), Intensive surveys of the Azores Front: 2. Inferring the geostrophic and vertical velocity fields, *J. Geophys. Res.*, *101*(C7), 16,291–16,303, doi:10.1029/96JC01144.

Rudnick, D. L., and J. R. Luyten (1996), Intensive surveys of the Azores Front: 1. Tracers and dynamics, *J. Geophys. Res.*, *101*(C1), 923–939, doi:10.1029/95JC02867.

Shepard, D. (1968), A two-dimensional interpolation function for irregularly-spaced data, in *Proceedings of the 1968 23rd ACM National Conference*, pp. 517–524, Assoc. of Comput. Mach., N. Y., doi:10.1145/800186.810616.

Spaulding, R. S., M. D. DeGrandpre, J. C. Beck, R. D. Hart, B. Peterson, E. H. De Carlo, P. S. Drupp, and T. R. Hammar (2014), Autonomous in situ measurements of seawater alkalinity, *Environ. Sci. Technol.*, *48*(16), 9573–9581, doi:10.1021/es501615x.

Strub, P. T., P. M. Kosro, and A. Huyer (1991), The nature of the cold filaments in the California Current System, *J. Geophys. Res.*, *96*(C8), 14,743–14,768, doi:10.1029/91JC01024.

Sutton, R. T., H. Maclean, R. Swinbank, A. O'Neill, and F. W. Taylor (1994), High-resolution stratospheric tracer fields estimated from satellite observations using Lagrangian trajectory calculations, *J. Atmos. Sci.*, *51*(20), 2995–3005, doi:10.1175/1520-0469(1994)051<2995:HRSTFE>2.0.CO;2.

Taylor, J. A. (1992), A global three-dimensional Lagrangian tracer transport modelling study of the sources and sinks of nitrous oxide, *Math. Comput. Simul.*, *33*(5), 597–602, doi:10.1016/0378-4754(92)90157-C.

Viúdez, Á., R. L. Haney, and J. T. Allen (2000), A study of the balance of horizontal momentum in a vertical shearing current, *J. Phys. Oceanogr.*, *30*(3), 572–589, doi:10.1175/1520-0485(2000)030<0572:ASOTBO>2.0.CO;2.

Whitt, D. B., and L. N. Thomas (2013), Near-inertial waves in strongly baroclinic currents, *J. Phys. Oceanogr.*, *43*(4), 706–725, doi:10.1175/JPO-D-12-0132.1.

Wilkerson, F. P., and R. C. Dugdale (1987), The use of large shipboard barrels and drifters to study the effects of coastal upwelling on phytoplankton dynamics, *Limnol. Oceanogr.*, *32*(2), 368–382, doi:10.4319/lo.1987.32.2.0368.

Yamazaki, H., and R. Lueck (1990), Why oceanic dissipation rates are not lognormal, *J. Phys. Oceanogr.*, *20*(12), 1907–1918, doi:10.1175/1520-0485(1990)020<1907:WODRAN>2.0.CO;2.